analytical chemistry

Feature

Cite This: *Anal. Chem.* 2018, 90, 3639−3650

pubs.acs.org/ac

Dynamic Nuclear Polarization Opens New Perspectives for NMR Spectroscopy in Analytical Chemistry

Dynamic nuclear polarization (DNP) can boost sensitivity in nuclear magnetic resonance (NMR) experiments by several orders of magnitude. This Feature illustrates how the coupling of DNP with both liquid- and solid-state NMR spectroscopy has the potential to considerably extend the range of applications of NMR in analytical chemistry.

Bertrand Plainchont,[†] Pierrick Berruyer,[‡] Jean-Nicolas Dumez,[§] Sami Jannin,[‡] and Patrick Giraudeau*[,†,∥]

[†]Université de Nantes, CNRS, CEISAM UMR 6230, 44322 Nantes Cedex 03, France

[‡]Université Claude Bernard Lyon 1, CNRS, ENS de Lyon, Institut des Sciences Analytiques, UMR 5280, 5 Rue de la Doua, 69100 Villeurbanne, France

[§]Institut de Chimie des Substances Naturelles, CNRS UPR 2301, Univ. Paris Sud, Université Paris-Saclay, 91190 Gif-sur Yvette, France

[∥]Institut Universitaire de France, 75005 Paris, France

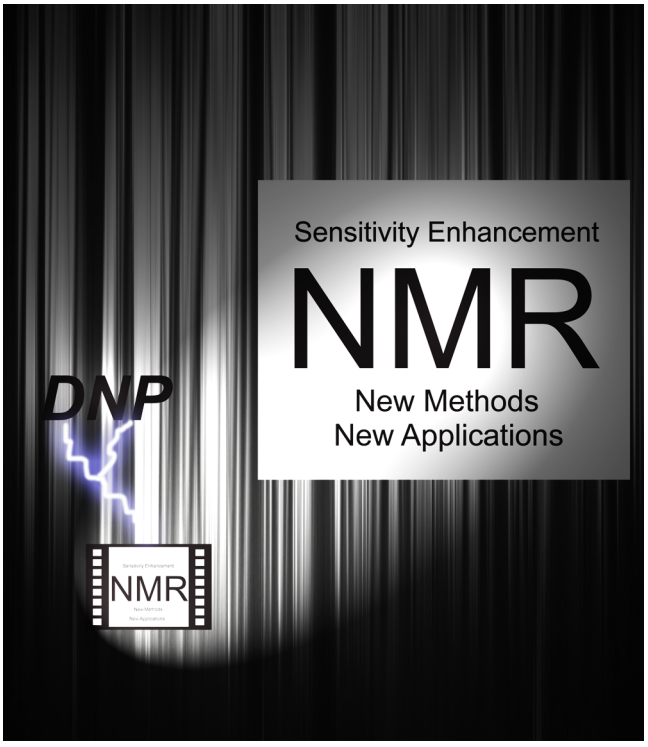

Dr. Bertrand Plainchont

Nuclear magnetic resonance (NMR) spectroscopy is a central tool in a broad range of analytical processes thanks to its high versatility, its nondestructive character, and its ability to provide both structural and quantitative information with a high level of confidence. Analytes ranging from small organic molecules to larger systems like proteins can be studied by NMR in a broad variety of samples in the liquid or solid state and even *in vivo*. The applications of NMR spectroscopy encompass highly diverse fields such as structure elucidation in organic chemistry, pharmaceutical and natural-product sciences, complex mixture analysis, structural biology, and material sciences.

NMR spectroscopy is potentially highly informative because it allows one to investigate compounds at an atomic-level, providing both structure and dynamics information. It is well recognized as a quantitative tool since the detected signal is directly proportional to the number of resonating nuclei, but the major drawback of NMR is its intrinsic low sensitivity. The minimal accessible concentration in solution is in the micromolar range for ^{1}H experiments at high field.

The sensitivity of NMR has been considerably improved with the increase of the magnetic field strength and, for solutions, with the advent of cryogenically cooled probes.[1] However, increasing the magnetic field is not straightforward and comes with high equipment costs. For solids, higher spinning frequencies have also improved the sensitivity allowing proton detected experiments under fast magic angle spinning (MAS) NMR.[2,3] However, the sensitivity of conventional NMR remains a limitation for many systems of interest.

The field of NMR is experiencing a major paradigm shift, with the advent of "hyperpolarization" techniques capable of producing nuclear spin polarization far beyond thermal equilibrium values and thus increasing the sensitivity by orders of magnitude, resulting in dramatic signal enhancements. The different hyperpolarization approaches that have been developed rely on spin-exchange optical pumping of noble gases (SEOP),[4] on the use of para-hydrogen induced polarization (PHIP),[5] of chemically induced dynamic nuclear polarization (CIDNP),[6] but dynamic nuclear polarization (DNP)[7] is probably the most general and efficient method in the hyperpolarization family. On the basis of the transfer of polarization from electrons to nuclei through microwave irradiation in a magnetic field, DNP has shown great potential to boost the sensitivity of both solid-state and liquid-state NMR detection, opening a broad array of

Published: February 26, 2018

DOI: 10.1021/acs.analchem.7b05236
Anal. Chem. 2018, 90, 3639−3650

applications that were not accessible to NMR so far for sensitivity reasons.

The purpose of this Feature article is to make accessible the different aspects of DNP NMR for a broad audience of chemists. The general concepts of DNP are briefly introduced, followed by a section dedicated to its practical implementation, including hardware and sample preparation aspects, and focusing on its use as an analytical tool. For advanced readers, an additional section is dedicated to the most recent methodological developments in this constantly growing field. The last section is devoted to an overview of recent applications in the field of analytical chemistry. Notably we illustrate how DNP has made it possible to observe signals that could not be observed with conventional NMR, giving access to essential structural information. A selection of promising results obtained on challenging systems illustrates that recent and future methodological developments could pave a way to new fields of research and application.

PRINCIPLES OF DNP

NMR Sensitivity. NMR has a low intrinsic sensitivity leading sometimes to unreasonably lengthy measurement times for low concentrated samples. This poor sensitivity is mainly due to a poor nuclear spin polarization in the magnetic field. This nuclear spin polarization can be seen in the case of a spin 1/2 either classically as the nuclear spin alignment along the magnetic field or quantum mechanically as a normalized difference in population between the spin states. The important feature of this polarization is that it is generally determined by a Boltzmann law at thermal equilibrium, giving

$$P = \tanh\left(\frac{\gamma \hbar B_0}{2k_B T}\right) \quad (1)$$

where γ is the gyromagnetic ratio of the spin, $\hbar$ is the reduced Planck constant, B_0 is the external magnetic field, k_B is the Boltzmann constant, and T is the temperature.

The NMR sensitivity is directly proportional to this polarization, and unfortunately this polarization is very small at conventional NMR conditions. Figure 1 represents in blue the nuclear spin polarization of protons for different typical operating magnetic fields. At an operating field of 14.1 T (corresponding to a middle-range NMR spectrometer), the nuclear spin polarization is only 0.000008 at 300 K for protons. The situation is even worse for nuclei with a lower gyromagnetic ratio. For example the ^{13}C nuclear spin polarization falls at 0.000002 at 14.1 T and 300 K.

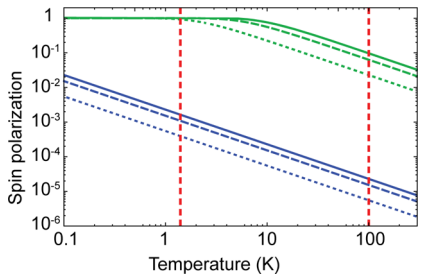

Figure 1. Electron (green) and ^1H (blue) spin polarization as a function of temperature, for magnetic fields of B_0 = 3.4 T (dotted lines), 9.4 T (dashed lines), and 14.1 T (solid lines). The red vertical lines indicate temperatures of 1.4 and 100 K.

From an analytical point of view, sensitivity becomes crucial when in some cases the desired information remains below the limit of detection. NMR experiments are generally repeated n times, until the signal-to-noise (S/N) ratio reaches a satisfactory value. This S/N ratio unfortunately only grows with $\sqrt{n}$, n being the number of repetitions of the experiment. In general, several seconds are typically needed between each scan to let the nuclear spin population relax to its equilibrium, which can lead to prohibitive acquisition durations, especially for low abundant and/or low gyromagnetic ratio (low-γ) nuclear spins. One may argue that infinitesimal concentrations could in principle be detected with increasingly long experimental times, but practical considerations evidently limit the overall durations of the NMR experiments to a few hours or a few days at most.

While eq 1 tells us that NMR sensitivity gets increased to a certain extent by applying higher external magnetic fields or lower experimental temperatures, even at the highest actual available magnetic field of 23.5 T the spin polarization of protons is only 0.000013 at 300 K.

Concept of DNP. The concept of DNP is almost as old as NMR since it was originally proposed by Overhauser in 1953.[7] He predicted that the NMR signal could be enhanced in metals by saturating the electron spin transitions of its conduction electrons. This hypothesis was then verified experimentally by Carver and Slichter on metallic lithium.[8]

The basic principle is that the higher level of polarization of the electron spins can be transferred to the surrounding nuclear spins upon microwave irradiation at (or near) the electron paramagnetic resonance (EPR) transitions. Figure 1 shows how the electron spin polarization is significantly higher than the one of the nuclear spins, reaching about 0.03 at 14.1 T and 300 K and almost unity at lower temperatures.

The DNP phenomenon exists in solids and in liquids. Four main different mechanisms (depending on the experimental conditions) can account for the DNP effect, namely, the Overhauser effect (OE), the solid effect (SE), the cross effect (CE), and the thermal mixing (TM). A detailed demonstration of these mechanisms is out of the scope of this Feature article; for more details the reader is invited to refer to excellent DNP reviews.[9−11] In solids, these DNP mechanisms usually strongly rely on nuclear spin diffusion; indeed, in a first step the transfer of polarization occurs from the electron spins to the nearby core nuclear spins, and in a second step, nuclear spin diffusion propagates this polarization further away toward the bulk nuclear spins.

IMPLEMENTATION OF DNP NMR

Experimental Approaches to DNP NMR. *DNP-MAS.* For 2 decades, the practical implementation of DNP had been limited to high-energy physics applications.[12] In the 80s, DNP has been increasingly used in static solid-state NMR experiments, for example, for the characterization of diamonds or coals,[13] but it is only in the 90s that the Griffin group demonstrated how DNP could truly become a beneficial technique for NMR by implementing it under MAS conditions.[14,15] Since then, considerable technological improvements have led DNP-MAS to become a mature technique. In 2009 Bruker Biospin released the first commercial version of the instrument, working at a field of 9.4 T. DNP-MAS is nowadays routinely performed at fields up to 14.1 and 18.8 T.

In practice, DNP-MAS is performed in an NMR probe with MAS capabilities that (i) can be cooled down to ∼100 K and that (ii) is equipped with a waveguide and beam launcher enabling

DOI: 10.1021/acs.analchem.7b05236
Anal. Chem. 2018, 90, 3639−3650

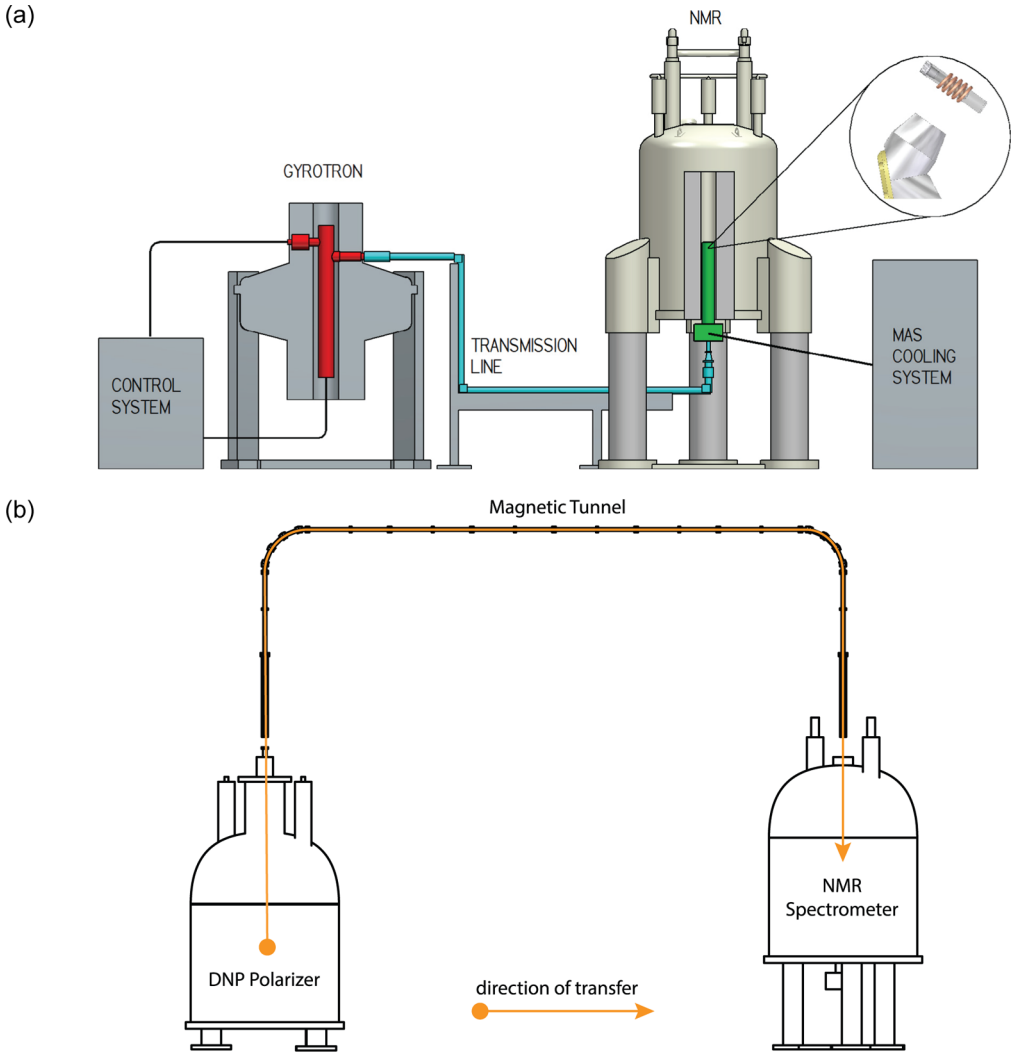

Figure 2. Schematic representation of experimental systems for (a) DNP-MAS NMR consisting of a gyrotron microwave source (gyrotron tube in red), a microwave transmission line (cyan), and an NMR spectrometer equipped with a low-temperature MAS probe (green) and (b) dissolution DNP NMR consisting in a cryostat (DNP polarizer), a transfer line with a magnetic tunnel, and an NMR spectrometer equipped with a liquid probe. The figure is reprinted with permission from ref 29 (Copyright 2016 Elsevier) and adapted in part from ref 20 (Copyright 2015 American Institute of Physics).

microwave irradiation of the sample under MAS conditions. The continuous wave irradiation is generated by an external gyrotron whose frequency is close to the electron spin resonance frequency in the magnet where the NMR experiment is performed. The microwave irradiation travels through a corrugated waveguide coupled to the NMR probe as can be seen on Figure 2a. The sample placed in the low-temperature MAS probe rotates about the magic angle at about 10−40 kHz (depending on the probe performances) and the typical operating temperature is 90−110 K.[11] Additional accessories for temperature and microwave control are included in the experimental setting. The in situ character of this experimental setting makes it compatible with most conventional solid-state NMR experiments. In particular, the approach is fully compatible with 2D NMR spectroscopy. However, the applicability of DNP-MAS may be limited by resolution losses caused by line broadening.

Dissolution DNP. For the study of liquid-state samples, the most popular method is dissolution DNP (d-DNP) that has been proposed in 2003 by Ardenkjaer-Larsen et al.[16] The apparatus used to perform d-DNP is presented in Figure 2b. The sample is placed in the DNP polarizer that consists mainly in a magnet, a cryostat, and a microwave source so that the DNP part of the experiment is first performed in the solid state at a relatively low external magnetic field (between 3 and 7 T[16−19]) and at a low temperature (between 1.2 and 4.2 K). Under such conditions, the spin polarization of the electron spins approaches unity. DNP is performed with low power microwave irradiation (typically 100 mW) on frozen samples that are subsequently rapidly melted and dissolved in a superheated solvent (generally water) by a dissolution device. The hyperpolarized liquid sample is then transferred either manually or automatically through a capillary ideally enclosed in a magnetic "tunnel" to minimize the losses of hyperpolarization.[20] The capillary can be connected to an injection device that either fills the NMR tube placed in an NMR magnet, or injects the solution in a phantom or living animal placed in an MRI scanner. Finally in both cases a liquid-state detection is performed. An additional multisample system has been proposed by Batel et al.[21] to perform a series of experiments.

In regards the solid-state part of this two-magnet approach, the transfer of polarization from electrons to nuclei other that ^{1}H can be done either directly or mediated by ^{1}H. The direct polarization approach suffers from long buildup times when

DOI: 10.1021/acs.analchem.7b05236
Anal. Chem. 2018, 90, 3639−3650

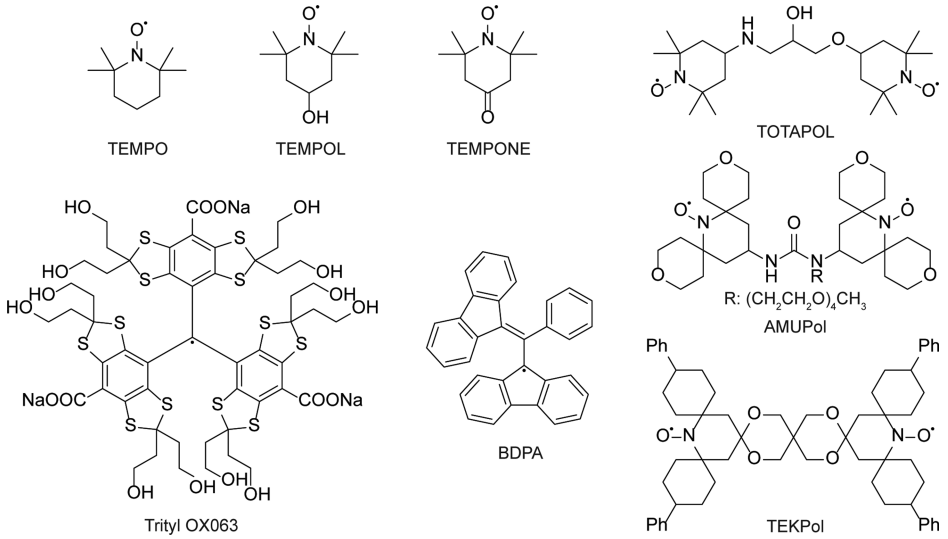

Figure 3. Chemical structures of radicals commonly used in DNP NMR experiments.

working with low-γ nuclei. By transferring polarization from the electron spins to protons, followed by cross-polarization (CP) to low-γ nuclei, the DNP process can be greatly accelerated, leading to dilute samples and to higher levels of polarization in shorter times.[22,23]

The d-DNP experiment has the advantage that the sensitivity enhancement not only comes from the DNP process itself but also from the temperature jump between polarization and detection. However, the main drawback of d-DNP is that, once in the solution state, the hyperpolarization decays with the nuclear spin−lattice relaxation time T_1 of the nuclear spins of interest. The DNP enhancement is thus available for a time on the order of a few seconds to minutes for nuclei with longer relaxation times. Therefore, the dissolution and transfer speeds are critical factors impacting the final sensitivity. In addition, the irreversible dissolution process makes d-DNP a single-shot technique that is not compatible with conventional 2D NMR experiments.

A d-DNP setting (HyperSense) is commercially available since 2005 from Oxford Instruments, and General Electrics launched in 2011 a system (SpinLab) that yields sterile samples and is adapted to clinical applications. The vast majority of the studies involving d-DNP have been in the field of preclinical and more recently clinical imaging[24] while applications to analytical chemistry have been more limited.

Other approaches have been considered to obtain solutions hyperpolarized by DNP, with the aim of enabling multishot experiments. For example, Joo et al. proposed the implementation of in situ liquid-state DNP at 90 K.[25] In this case the sample is melted thanks to a laser pulse and can be refrozen thereafter. There is no additional dilution and no transfer of the sample and the experiment can be recycled, making it compatible with multidimensional experiments. More recently a similar in situ rapid melt approach has been described by Sharma et al. by using hot nitrogen instead of laser pulses.[26] Other approaches relying on sample shuttle DNP with a dual center magnet[27] or in situ temperature-jump DNP[28] have also been described in the literature.

Concerning the study of liquid samples, some research groups have also considered performing DNP directly in the liquid state either in situ[30−33] or with a two-field shuttle DNP spectrometer.[34] The instrumentation is more demanding and the polarization transfer is much less efficient compared to DNP in the solid state. This part of the DNP area is still at the exploration stage in particular at high magnetic fields. Thus, there are not yet applications in the field of analytical chemistry.

Sample Preparation. When attempting to perform DNP experiments, particular care is needed with respect to the sample preparation. The sample needs to be doped with unpaired electrons that are used as polarizing agents. In general, these polarizing agents are stable free radicals that are simply added to the analytes, often dissolved in a glass forming solvent mixture upon freezing. It is usually critical that the radical solution forms a homogeneous glass upon freezing (and not ice crystals) to ensure a statistical distribution of the polarizing agents and avoid their aggregation. A homogeneous glassy DNP sample quasi-systematically leads to a best DNP efficiency. Experimentally, the polarizing agents are generally dissolved in an aqueous matrix D_2O/H_2O with a cryo-protectant such as glycerol-d_8 or DMSO-d_6;[35] alternatively, organic solvents such as tetrachloroethane can also be used.[36] Depending on the nature of the analytes, the latter can be dissolved in the radical solution[35] or impregnated to preserve the structure of the solid sample.[37]

Figure 3 shows some examples of commonly used radicals.[38−41] The typical concentration ranges from 5 to 50 mM, and the choice of the radical depends on various factors such as its performances in a given condition or in a particular solvent. The synthesis of effective polarizing agents has focused an important attention and the field is constantly under development.[42−45] Optimized polarizing agents for higher magnetic field (≥18.8 T)[46,47] is an important field of future development for DNP-MAS as the performance of current polarizing systems strongly decreases at higher magnetic field.

DNP Efficiency: Enhancement Factor. The DNP efficiency can be described by a polarization enhancement factor ε that is equal to the polarization attained with DNP (P_{DNP}) divided by the thermal equilibrium polarization (P_{TE}):

$$\varepsilon = \frac{P_{DNP}}{P_{TE}} \quad (2)$$

In the solid state with a static sample, ε is theoretically limited to the ratio of polarizations between the electron spin S and the nuclear spin I, which, in the high temperature approximation, is simply the ratio of the gyromagnetic ratios:

DOI: 10.1021/acs.analchem.7b05236
Anal. Chem. 2018, 90, 3639−3650

$$\varepsilon \leq \frac{P_S}{P_I} = \frac{\gamma_S}{\gamma_I} \quad (3)$$

In static conditions, this DNP enhancement factor is limited to 660 for protons and 2615 for ^{13}C when the thermal equilibrium signal is measured in the same conditions as where DNP is performed. Under MAS conditions, the nuclei can be in a depolarized state in the absence of microwave irradiation leading to an apparent greater ε than the maximum theoretically attainable in static conditions.[48,49]

In the case of d-DNP, the enhancement factor can reach high values because the sample undergoes a temperature jump from liquid-helium temperature to room temperature as well as potentially a magnetic field change. In practice, the d-DNP method can therefore lead to spectacular observed signal enhancements up to 50000.[22,50] However, the gain in sensitivity cannot only be limited to the sole evaluation of ε that does not take into account the many factors influencing the performance of hyperpolarization.

RECENT METHODOLOGICAL DEVELOPMENTS IN DNP NMR

This section will be of interest for advanced readers who would like to have more details on the most recent methodological advances in DNP-NMR.

Developments in DNP-MAS NMR. *Ultralow-Temperature DNP-MAS.* Currently, DNP-MAS NMR experiments are mainly performed at sample temperatures of about 100 K, using cold nitrogen gas to pneumatically spin and cool the sample. Lee et al. recently showed how cryogenic helium gas could be used to reach stable and fast spinning for sample temperatures down to 30 K using a home-built cryostat.[51] On model systems under classical DNP-MAS NMR conditions at 9.4 T and 110 K, ^{1}H DNP enhancements of ∼300 are commonly reached. When decreasing the temperature at 55 K, enhancements of ∼680 are observed for protons. In another publication by Thurber et al., the authors reported enhancement factors for cross-polarized ^{13}C NMR signals in the 100−200 range with DNP at 25 K.[52]

High-Temperature DNP-MAS. On the contrary, others have been interested to perform DNP-MAS at a higher temperature. Low-temperature DNP-MAS prevents the massive adoption of DNP-MAS for protein structural studies as these biomolecules usually exhibit broad unresolved signals at temperatures around 100 K. In 2012, Oschkinat and co-workers have obtained an improved resolution of a deuterated SH3 sample hyperpolarized with a TOTAPOL solution with an enhancement of about 10 at 180 K.[53] Later, Lelli et al. discovered that TEKPOL dissolved in orthoterphenyl allows one to maintain high DNP enhancements at high temperature.[54] The authors reported a ^{1}H enhancement of 80 at 240 K and 15 at room temperature. It was attributed to the relatively high glass transition temperature (T_g = 243 K) of orthoterphenyl. It allowed them to study the dynamics of Ambroxol and Ibuprofen.

Very Fast MAS DNP. In 2015, Chaudhari et al. reported the first results with a DNP-MAS probe using a 1.3 mm rotor. At approximately 110 K, the authors were able to reach a sample spinning frequency of up to 40 kHz, far over the MAS rate of 15 kHz obtain with the 3.2 mm rotor typically used for DNP-MAS.[55] They reported that the DNP enhancement for AMUPOL quickly increases when increasing the MAS frequency and then stabilizes at its maximum value. Later, they studied the MAS dependence of BDPA dissolved in orthoterphenyl and obtained the highest known enhancement of over 100 when working at high field (18.8 T) and 40 kHz MAS rate.[56] This achievement was made possible through the unexpected discovery that enhancement factors of BDPA increase rapidly with increasing MAS rates. The authors proposed a theoretical description by a source-sink spin diffusion model for polarization transfer that is capable of explaining the experimental observations.

Solvent Suppression Methods. Under DNP-MAS conditions, the addition of solvated radicals to the sample yields NMR spectra that may present large solvent signals and that can obscure ^{1}H or ^{13}C signals of interest from the analyte. Yarava et al. introduced two methods to suppress the solvent signals depending on the sample preparation.[57] A method based on relaxation filters led to efficient solvent suppression with minimal signal losses for impregnated powders. In the case of homogeneous frozen solutions, short cross-polarization contact times can be used to eliminate solvent signals. In parallel, Lee et al. proposed two methods for solvent suppression named forced echo dephasing experiment (FEDex) and transfer of populations in double resonance echo dephasing (TRAPDORED) that both work through the reintroduction of the heteronuclear dipolar interactions between ^{13}C spins from the DNP solvent.[58] The utility of these methods has been demonstrated for analytes in frozen solution as well as in powdered form.

Developments in d-DNP NMR. *Accelerating Sample Transfer after Dissolution.* In the quest to make the method accessible to nuclei with shorter relaxation times, hardware optimization plays a crucial role. After dissolution, the transfer of the liquid sample to the magnet dedicated to the experiment must be as fast as possible. Complex sample motions such as convection or gas bubbles due to fast injection have to be taken into account because they are not only detrimental to signal line widths but also to the implementation of gradient-based spatial encoding experiments. A strategy proposed by Bowen et al. is to maintain a high gas pressure on the liquid sample during acquisition by using a multiport valve and a loop for injection.[59] Another approach is to perform sample delivery by a high-pressure liquid. Chen et al. have demonstrated that this flow injection process shows better performance than a gas-driven injection.[60]

Coupling with Ultrafast 2D NMR. One of the main limitations of d-DNP is its single-scan nature arising from its irreversible character. Conventional 2D NMR experiments cannot be performed with d-DNP enhanced polarization, except in specific cases where a small-angle excitation can be employed.[61] Among the methods that have been introduced for fast multidimensional NMR, the ultrafast (UF) 2D NMR is one general approach compatible with d-DNP experiments as demonstrated by Frydman and co-workers.[62,63] UF 2D NMR relies on a spatial encoding of NMR interactions thanks to a combination of chirp pulses with magnetic field gradients, followed by an acquisition performed with an echo planar spectroscopic imaging scheme. UF 2D NMR makes it possible to collect a 2D data set in a single scan, thus providing an appealing solution to the irreversibility of d-DNP. Recently, the ultrafast 2D NMR methodology has been adapted by Guduff et al. to record ^{13}C diffusion-ordered NMR spectroscopy (DOSY) experiments from DNP hyperpolarized samples within a single scan.[64] DOSY are collected in a single scan by spatial parallelization, in which different virtual slices undergo different diffusional attenuations.

Hyperpolarized Solution Purity. In some applications of d-DNP, the issue of the presence of free radicals in solution is raised. For example in the study of proteins, one may prevent any

DOI: 10.1021/acs.analchem.7b05236
Anal. Chem. 2018, 90, 3639−3650

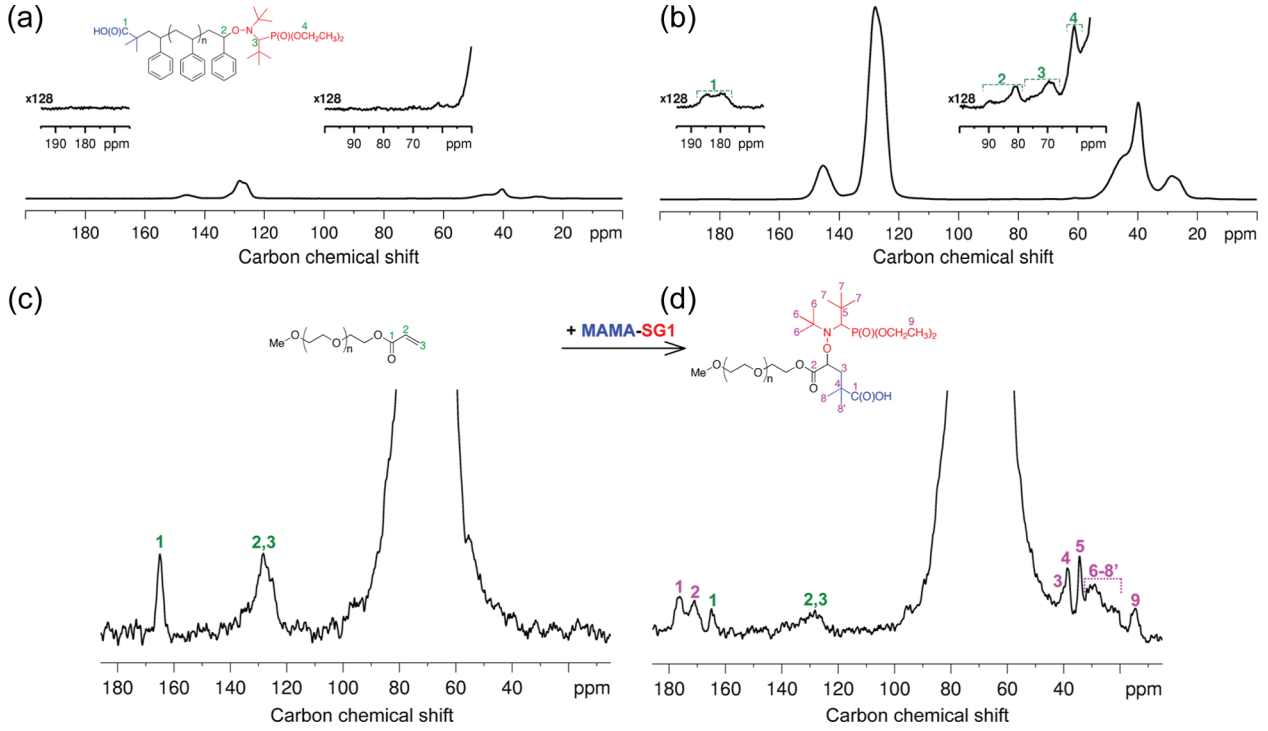

Figure 4. (upper) ^{13}C CPMAS SSNMR spectra of a living PS sample (M_n = 13 500 g mol^{-1}) obtained (a) without or (b) with DNP (at 285 and 105 K, respectively). The sample in part b was doped with 0.5 wt % bCTbK. In both cases 26 624 scans were used (~15 h), and intensity scales are identical. (lower) ^{13}C DNP CPMAS SSNMR spectra of an acrylate-terminated PEO sample (M_n = 35 000 g mol^{-1}) obtained before (c) and after (d) the 1,2 intermolecular radical addition with MAMA-SG1. In both cases, 0.5 wt % bCTbK and 1600 scans were used (~13 h). In part d, NMR signals due to both the acrylate PEO and the living PEO samples can be observed, implying that the reaction was not complete. The figure and caption are reproduced from ref 83 (Copyright 2013 American Chemical Society).

interaction having a potential side effect. For *in vivo* MRI experiments, the presence of additional products in the injected solution is obviously undesirable. To obtain solution purity, some methods depending on the nature of the radicals have been proposed to eliminate the radicals by precipitation followed by filtration,[65−67] by solvent extraction,[68] or by chemical quenching.[69] More recently, Gajan et al. have shown the high polarizing efficiency at very low temperatures (1.2 and 4.2 K) of hybrid polarizing solids (HYPSOs), a family of hybrid organosilica materials in which radicals are covalently linked to the pore channels and homogeneously randomly distributed in the mesostructured silica matrix.[70] After polarization, radical-free hyperpolarized solutions can be easily obtained by physical retention during dissolution.

Sustaining Hyperpolarization in Solution. A way to prolong the lifetime of the hyperpolarization in solution is to use the so-called long-lived states[71] (LLS) that are nuclear spin configurations delocalized on two or more coupled spins. LLS have unusually long relaxation times that make it possible to benefit from hyperpolarization for NMR experiments in a relatively longer amount of time after the dissolution step. In 2009, Vasos and co-workers demonstrated on the dipeptide Ala-Gly that the lifetime of the LLS involving the two nonequivalent Hα protons of glycine was seven times longer than their spin−lattice relaxation time constant.[72] Examples of NMR applications of LLS in association with d-DNP are presented in the following section.

Toward Transportable Hyperpolarization. In a recent publication, Ji et al. have described a method that extends the hyperpolarization lifetime before dissolution and enables the transportation of hyperpolarized samples.[73] The hyperpolarization can be stored in a frozen state during several hours and the sample analyzed at remote NMR or MRI sites. Hyperpolarized samples of alanine and glycine have been stored during 16 h and enhancement factors up to 1700 were measured after dissolution.

RECENT EXAMPLES OF DNP NMR SPECTROSCOPY APPLICATIONS

Thanks to the aforementioned developments, DNP-NMR has reached a significant level of maturity, thus paving the way toward a broad range of applications. Some of the most recent are mentioned below, focusing on those which we believe could have a strong impact in the field of analytical chemistry.

Applications of DNP in MAS NMR. The pioneering applications of DNP in the solid state were mostly devoted to structural biology. Recently, new biological insights were obtained on highly complex systems like HIV-1 virus capsids,[74] needle-like structures from bacterial secretion systems,[75] or in-cell proteins.[76]

In the analytical chemistry context, DNP allows to probe the surface of materials, giving access to surface species otherwise diluted in bulk spectra. DNP-NMR is particularly useful when the amorphous nature of the sample prohibits the use of diffraction-based methods. DNP-NMR also gives access to information that is not accessible by NMR alone because of the low concentration, low abundance, or low-γ or in the case of quadrupolar nuclei.

Surface Probing of Materials. In 2010, the DNP surface enhanced NMR spectroscopy (DNP-SENS) technique was introduced to selectively probe the surface or surface-bound species of materials.[37,77] For example, surface−metal interactions were found between an Ir(I) hydrogenation catalysts anchored

DOI: 10.1021/acs.analchem.7b05236
Anal. Chem. 2018, 90, 3639−3650

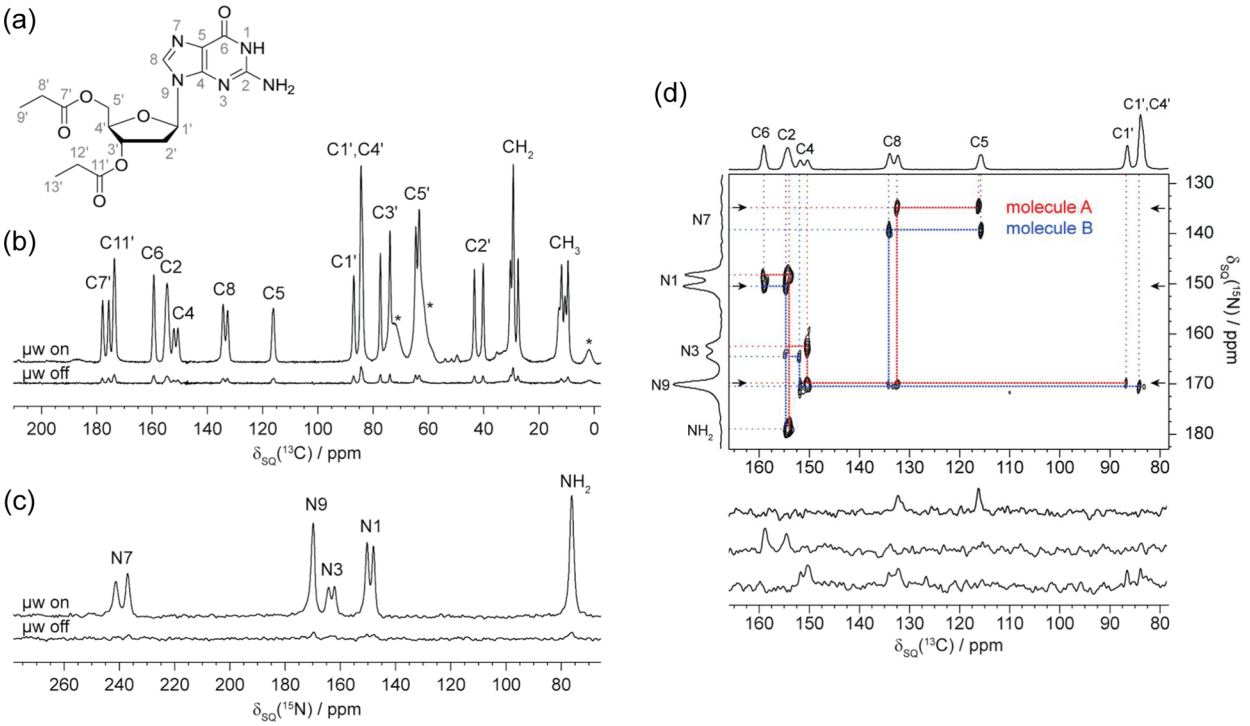

Figure 5. (a) Chemical structure of $dG(C3)_2$ and ^{13}C (b) and ^{15}N (c) CPMAS spectra. Asterisks (*) indicate glycerol and silicon grease (from sample synthesis and preparation). (d) $^{15}N-^{13}C$ DCP-HETCOR spectrum. $^{15}N-^{13}C$ polarization transfer was achieved by adiabatic transfer (APHH–CP) with a contact time of 7 ms. The spectrum was recorded in ~25 h. The spectral width in the indirect dimension was optimized such that N7 and NH_2 resonances are folded on the respective opposite side of the spectrum. Cross sections are shown below the spectrum, taken at the positions indicated by arrows. Molecules A and B refer to the two distinct molecules contained in the asymmetric unit cell. The figure and caption are reproduced with permission from ref 86 (Copyright 2015 American Chemical Society).

on a silica surface and are believed to be an explanation for the difference of catalytic activity between the supported Ir(I) catalyst and its molecular analogue.[78]

DNP-SENS has been used for the description of reaction intermediates for supported metathesis catalysts. Ong et al. showed that isotopic labeling and DNP SENS allow the direct determination of the bond connectivity and the measurement of the carbon–carbon bond distances in metallacycles, which are the cycloaddition intermediates in the alkene metathesis catalytic cycle.[79] In this case, the observation of ^{13}C correlations in 2D refocused INADEQUATE and 2D homonuclear dipolar recoupling POSTC7 experiments highlighted that DNP could help understanding the slow initiation and deactivation steps in the heterogeneous metathesis catalysts.

More recently, it has been demonstrated that DNP-SENS can be used to obtain the tridimensional structure of organometallic complexes anchored to surfaces.[80] Rotational echo double resonance (REDOR) experiments were performed and used in combination with extended X-ray absorption fine structure (EXAFS).

Aluminas are highly used as catalysts or catalyst supports in industry. Lee et al. have used MAS NMR to selectively probe on the one hand the bulk of γ-alumina nanoparticles and on the other hand their surface thanks to DNP.[81] The authors have shown that there were no detectable hydroxyl groups in the bulk of the material and demonstrated by multiple-quantum magic angle spinning (MQMAS) that pentacoordinated Al^{3+} ions are only observed in the first surface layer.

Heterogeneous solid Brønsted catalysts are other examples with industrial relevance. Perras et al. have studied Brønsted acid sites at the surface of oxide materials at natural abundance by ^{17}O DNP SENS.[82] ^{17}O is a quadrupolar nucleus (spin-5/2) and has an extremely low natural abundance of 0.038%. The authors directly probed the Brønsted acidity of surface hydroxyls in silica and silica–alumina materials. ^{17}O spectra with ^{1}H decoupling have been acquired using the PRESTO-QCPMG technique (phase-shifted recoupling effects a smooth transfer of polarization quadrupolar Carr–Purcell–Meiboom–Gill). Additionally, O–H bond lengths have been measured with subpicometer precision giving a direct structural gauge of the lability of protons.

Structure Elucidation. Polymers are challenging because chain ends give intrinsically diluted NMR signals that are not detected by conventional MAS NMR. Ouari et al. demonstrated that DNP permits the detection and precise structural elucidation of chain ends that are essential to control polymer reactivity.[83] They have studied two examples of synthetic functional polymers, living polystyrene (PS) and poly(ethylene oxide) (PEO) samples obtained via NMP and 1,2-intermolecular radical addition, respectively, in the presence of the MAMA-SG1 initiator. The ^{13}C spectra in Figure 4a,b give an estimation of the sensitivity gain achieved by DNP by comparing the S/N ratio of the two spectra. For the signal at 128 ppm, the sensitivity gain is approximately 13. As a consequence, this spectrum was obtained in 15 h. Without DNP the same spectrum would require signal accumulation for more than 100 days. The ^{13}C spectra in Figure 4c,d reveal the presence of chain end signals that enable verification of polymer functionalization. The signals of the acrylate PEO precursor in Figure 4d reveal that the reaction was not complete.

The success of structure characterization of polymorphs of molecules is usually based on *ab initio* crystal structure prediction (CSP), infrared spectroscopy, and powder X-ray diffraction

DOI: 10.1021/acs.analchem.7b05236
Anal. Chem. 2018, 90, 3639–3650

(PXRD) that are currently used to characterize organic powders, but they only provide partial details on atomic and molecular structure. In a recent study, Pinon et al. used DNP-MAS NMR to record $^{1}H-^{13}C$ and $^{1}H-^{15}N$ HETCOR, and $^{13}C-^{13}C$ INADEQUATE spectra obtained at natural isotopic abundance in reasonable times.[84] In this example, the structure of three polymorphs and one hydrated form of the asthma drug molecule theophylline were elucidated.

Rossini et al. demonstrated the application of DNP to the atomic-level characterization of active pharmaceutical ingredients (API) in commercial pharmaceutical formulations by the impregnation method.[85] The gently ground tablets were impregnated with solutions containing biradical polarizing agents, and all liquids were chosen so that the API was minimally perturbed. The authors studied four different commercial formulations of the antihistamine drug cetirizine dihydrochloride (between 4.8 and 8.7 wt % API). DNP allowed the rapid acquisition of 1D and 2D ^{13}C and ^{15}N MAS NMR spectra of the formulations at natural isotopic abundance while preserving the microstructure of the API particles. Signal enhancements between 40 and 90 were observed at 105 K. In addition, API–excipient interactions were observed in $^{1}H-^{15}N$ correlation spectra, revealing direct contacts between povidone and the API.

A new exciting application is the crystal structure determination of molecular assemblies by means of DNP-enhanced NMR crystallography. Märker et al. completed the entire *de novo* ^{13}C and ^{15}N resonance assignment at natural abundance of a 2′-deoxyguanosine derivative (Figure 5a) presenting two different molecules in the asymmetric crystallographic unit cell.[86] DNP-MAS NMR correlation experiments with high spectral resolution led to an unambiguous assignment of both conformers that was globally in agreement with previously published results based on theoretical calculations. A DNP enhancement of a factor 11 was observed in 1D spectra (Figure 5b,c). A 2D through-bond $^{13}C-^{13}C$ INADEQUATE spectrum was recorded for ^{13}C assignment, and a 2D $^{15}N-^{13}C$ double CP based heteronuclear correlation experiment (Figure 5d) was recorded for ^{15}N assignment.

Märker et al. studied the 3D structure of self-assembled cyclic diphenylalanine peptides at natural abundance.[87] Aromatic interactions between the phenyl rings are the main driving forces in self-assembly, with both parallel and perpendicular π-stacking occurring. The authors used dipolar recoupling pulse sequence S_3 and $[S_3]$ which facilitate the recoupling of carbons with large chemical shift anisotropy, such as carbonyl and aromatic carbons. They detected and measured long-range ^{13}C internuclear distances up to approximately 7 Å. This example highlights that DNP-MAS NMR is a powerful tool for the analysis of one of the most important noncovalent interactions by observing π-stacking through $^{13}C-^{13}C$ correlation spectra.

Exotic nuclei. Kobayashi et al. demonstrated the acquisition of ^{195}Pt spectra with spectral widths reaching ~10000 ppm by combining DNP enhancement with broadband cross-polarization and CPMG detection.[88] They characterized the coordination of atomic Pt species supported within the pores of metal–organic frameworks (MOFs). The spectra served to separate signals from cis- and trans-coordinated atomic Pt^{2+} species supported on the UiO-66-NH_2 MOF. Additionally, the data revealed the dominance of kinetic effects in the formation of Pt^{2+} complexes and the thermodynamic effects in their reduction to nanoparticles.

Kobayashi et al. also used DNP to enhance the wide-line ^{207}Pb solid-state NMR spectra of lead white pigment.[89] DNP allowed one to detect the formation of a lead soap which is a degradation product implicated in the deterioration of lead-based oil paintings. The existence of two Pb sites was shown, corresponding to the carbonate and hydroxide layers.

Applications of d-DNP in Liquid NMR. Dissolution DNP has reached a lower level of maturity in terms of applications to chemistry. d-DNP has opened many perspectives in preclinical imaging, which represent the vast majority of its applications at the time of writing.[90,91] While these applications are out of the scope of this review, several recent studies have also highlighted the great potential of d-DNP in analytical chemistry, as described in the following paragraphs.

Protein–Ligand Interaction. In the study of protein–ligand interactions, the classical water-ligand observed via gradient spectroscopy (water-LOGSY) experiment, involving saturation of bulk H_2O and transfer to bound ligands, suffers from low sensitivity and false-positives caused by aggregated or denatured proteins. Chappuis et al. showed that sensitivity could be boosted by injecting hyperpolarized water into solutions of proteins and ligands.[92] Additionally, with this method the integrity of the protein can be verified, and false positives due to nonspecific binding to aggregated proteins can be discarded.

Min et al. demonstrated the observation of the transfer of spin polarization from hyperpolarized ligands to protein on the example of benzamidine with the serine protease trypsin.[93] This effect can be used for screening in drug discovery and is an alternative to the widely used saturation transfer difference (STD) NMR experiment. Classical methods like STD, involving selective saturation of target protons and relying on spin diffusion to propagate saturation to bound ligands, are limited by their low sensitivity because the target protein, and in some case the ligand, are difficult to obtain or suffer from a low solubility. In this type of application, d-DNP has the advantage to help override the sensitivity issue.

Buratto et al. proposed a technique for drug screening using LLS.[94] In this application, after the dissolution process, the hyperpolarization could be converted into LLS and the contrast between the lifetimes of the LLS of the bound and free forms was exploited.

Reaction Monitoring. A challenging task in the study of (bio)chemical reactions is the characterization of intermediate species that form as the reaction occurs. Since these species are often short-lived and low-concentrated, they are difficult to detect and enhancing the sensitivity of NMR detection through d-DNP can be an efficient alternative in this field. Several examples, mainly in the case of ^{13}C NMR, showed that in addition to providing insights into reaction mechanisms, this strategy also gives access to kinetic information.

For instance, Lee et al. demonstrated a strategy using d-DNP to detect intermediate species during the anionic polymerization of styrene.[95] Starting from hyperpolarized monomers, signals from polymers could be observed during reaction because hyperpolarization was continuously incorporated at the site of monomer addition, so the active site of the growing polymer chain could be selectively enhanced.

Several studies also showed the potential of d-DNP to study enzymatic kinetics.[96,97] As an example, Miclet et al. studied the kinetics of the enzymatic phosphorylation reaction of glucose to form glucose-6-phosphate by hexokinase.[98] The catalytic constant of the reaction was estimated with a simple model tailored for hyperpolarized systems that takes into account the

DOI: 10.1021/acs.analchem.7b05236
Anal. Chem. 2018, 90, 3639–3650

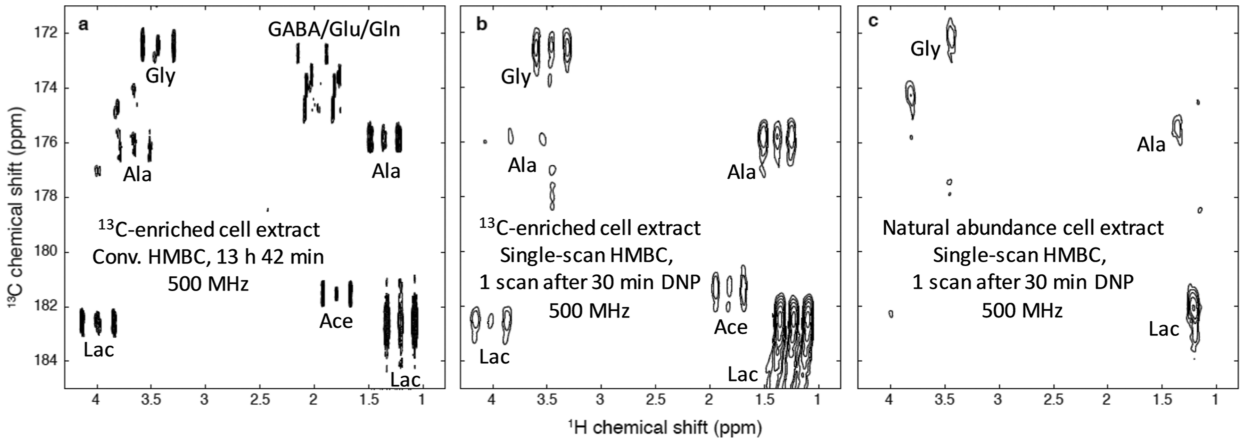

Figure 6. $^{1}H \rightarrow {}^{13}C$ HMBC-type spectra of extracts of SKBR3 human breast cancer cell lines. (a) Conventional HMBC spectrum, recorded in 13 h 42 min at 500 MHz with a cryogenic probe, on a partially enriched extract (~57 million extracted cells) dissolved in 700 μL of D_2O. (b) Hyperpolarized single-scan spectrum. The cell extract was dissolved in 200 μL of a mixture of H_2O/D_2O/glycerol-d_8 (2:3:5) with 25 mM TEMPOL and polarized for 30 min at 1.2 K and 6.7 T, and finally dissolved with 5 mL of D_2O. A fraction of 700 μL of the hyperpolarized sample was injected in a 500 MHz spectrometer equipped with a cryogenic probe where the spectrum was recorded in a single scan. (c) Same as part b but with a natural abundance extract (~113 million cells) obtained from the same SKBR3 cell line. Ace,acetate; Ala, alanine; GABA, γ-aminobutyrate; Gln, glutamine; Glu, glutamate; Gly, glycine; Lac, lactate. The figure and the caption are reproduced with permission from ref 103 (Copyright 2015 The Royal Society of Chemistry).

inhibition by the reaction product. In the same vein, Bornet et al. reported the creation of hyperpolarized LLS to monitor a slow enzymatic process that corresponds to the conversion of fumarate into malate.[99] In another example, after demonstrating the feasibility of the real-time monitoring of betaine aldehyde metabolism using a hyperpolarized choline analogue,[100] Allouche-Arnon et al. measured the reaction rate constants in successive enzymatic processes with a kinetic model designed for multireactions schemes.[101]

Metabolomics. While most d-DNP studies have reported the hyperpolarization of a single (and often labeled) molecule,[102] the hyperpolarization of complex mixtures is a much more recent concept. Nevertheless, it could open interesting perspectives in the growing field of metabolomics where NMR is mainly limited to ^{1}H detection, with heavily overlapped 1D spectra. ^{13}C NMR could be highly promising in this field, but its application to diluted and complex biological mixtures is not realistic for sensitivity reasons. In this context, Dumez et al. recently published a proof-of-concept paper showing that biological extracts could be efficiently hyperpolarized and detected by ^{13}C NMR after dissolution.[103] Natural abundance ^{13}C NMR spectra were acquired in a single scan by coupling d-DNP and CP, the latter being a key factor to efficiently hyperpolarize such diluted samples. High levels of ^{13}C spins hyperpolarization were obtained in complex systems like tomato extracts or human breast cancer cell lines. They also applied the ultrafast 2D NMR methodology to record heteronuclear correlation spectra on such extracts. Figure 6 shows an HMBC-type spectrum obtained in a single scan on both enriched and natural abundance breast cancer cell extracts. The actual limitation is that only quaternary carbons could be observed after dissolution and transfer due to a transfer time of several seconds. Nevertheless, the recent improvements in the reduction of the transfer time could circumvent this limitation. Hyperpolarized NMR of biological mixtures could then form a promising tool to improve the sensitivity of ^{13}C NMR metabolomics, and 2D spectroscopy would be a useful tool to separate overlapping resonances while providing useful assignment information.

Following this proof of concept, with the aim to demonstrate the analytical potential of the method for application to real studies involving large sample collections, a study on the experimental repeatability was performed by Bornet et al.[104] The detection of metabolites in tomato extracts by ^{13}C NMR at natural abundance was reported with a repeatability of 3.6% for signals above the limit of quantification and 6.4% for signals above the limit of detection. These results show that the analytical characteristics of d-DNP, in spite of a relatively complex hyphenated hardware, are compatible with the precision requirements of metabolomics.

Note that the repeatability could be further improved by the use of a reference method to account for potential variations in the polarization and dissolution processes. In a recent publication, Lerche et al. presented the implementation of an internal standard method for a reproducible quantitative analysis of ^{13}C-enriched metabolites.[105] To monitor metabolic pathway activities, cancer cells were grown with uniformly ^{13}C-labeled glucose and metabolites were extracted, hyperpolarized, and then analyzed by ^{13}C NMR. The metabolic patterns of prostate and breast cancer cells were investigated by this method.

CONCLUSIONS AND PERSPECTIVES

In this Feature article, we have attempted to provide a brief overview of the concepts and instrumental aspects of the different DNP approaches coupled to NMR, and we have proposed a selection of methodological progress and recent applications in analytical chemistry. Among other hyperpolarization techniques, DNP becomes more and more popular among the NMR community due to an increasing availability, although the accessibility of d-DNP equipment remains to be improved. Boosting the NMR signal with large enhancement factors allows one to considerably reduce the experimental time or to make accessible information that could not be retrieved with conventional NMR alone. The sensitivity gain permits the detection of low concentrated analytes or nuclei which suffer from poor sensitivity due to their low natural abundance, low gyromagnetic ratios, or large anisotropic interactions. As a result DNP has the potential to considerably increase the range of applications of NMR. While DNP-MAS NMR is already a technique which has reinforced the applicability of conventional MAS NMR by addressing previously unsolvable problems, the

DOI: 10.1021/acs.analchem.7b05236
Anal. Chem. 2018, 90, 3639−3650

applications of dissolution DNP are still at a preliminary stage. This is probably partly due to the absence of commercial equipment that would include the major recent developments in the field. Nevertheless, d-DNP has a great potential of application in analytical chemistry, as highlighted by recent proof-of-concept papers. In addition, the limitations inherent to its single-shot nature may be overcome by technological developments to speed up the dissolution and transfer process and by the use of UF 2D NMR for detection. Globally, the development potential for both methodologies goes hand in hand with a better understanding of the DNP mechanisms, a development of the instrumentation, and an optimization of the polarizing agents and the sample preparation. DNP is a highly valuable technique that deserves to become a standard feature of high-field NMR spectroscopy, paving a way to new horizons in analytical chemistry.

AUTHOR INFORMATION

Corresponding Author

*E-mail: patrick.giraudeau@univ-nantes.fr.

ORCID

Pierrick Berruyer: 0000-0003-1783-6034

Patrick Giraudeau: 0000-0001-9346-9147

Notes

The authors declare no competing financial interest.

Biographies

Bertrand Plainchont obtained his Ph.D. from the University of Reims Champagne-Ardenne (France) and performed postdoctoral research at University Paris-Sud (France). He is currently a postdoctoral research fellow at the University of Nantes, France. His research interests are computer-assisted structure elucidation and verification, the development of NMR experiments for the simplification of complex NMR spectra, and spin dynamics simulation. His current research focuses on hyperpolarized ultrafast 2D NMR for the analysis of complex mixtures.

Pierrick Berruyer received his Ph.D. in 2017 from the Ecole Normale Supérieure de Lyon (France) working on three-dimensional surface structure determination with DNP surface enhanced SSNMR. He also developed new methods and formulations for DNP-MAS.

Jean-Nicolas Dumez is a CNRS associate scientist at Université Paris Saclay (France). He received his Ph.D. in 2011 at the Ecole Normale Supérieure de Lyon (France) and then performed postdoctoral research 2011−2013 at the Weizmann Institute of Science (Israel) and at the University of Southampton (U.K). His current work focuses on methods development in solution-state NMR spectroscopy and, in particular, the analysis of complex mixtures of small molecules with increased speed and sensitivity.

Sami Jannin is a Professor at the Lyon 1 University in France whose field of expertise is centered around dissolution dynamic nuclear polarization. His research interests span from the development of new d-DNP and NMR methods and instrumentation to the exploration of new d-DNP enhanced applications.

Patrick Giraudeau is a Professor of Analytical Chemistry at the University of Nantes, France. He received his Ph.D. from the Univ. Nantes in 2008, followed by a postdoctoral research position 2008−2009 at the Weizmann Institute of Science (Israel). Patrick Giraudeau's research interests include the development of NMR methods for the accurate quantitative analysis of complex mixtures, with a specific focus on fast multidimensional NMR methods and their applications to analytical chemistry.

ACKNOWLEDGMENTS

This work was supported by the French National Research Agency (Grant ANR-17-ERC2-0011), the European Research Council under the European Union's Horizon 2020 Research and Innovation Programme (ERC Grant Agreement No. 714519/HP4all), the ENS-Lyon, the French CNRS, Lyon 1 University, and Nantes University.

REFERENCES

(1) Kovacs, H.; Moskau, D.; Spraul, M. *Prog. Nucl. Magn. Reson. Spectrosc.* **2005**, *46*, 131−155.
(2) Ishii, Y.; Tycko, R. *J. Magn. Reson.* **2000**, *142*, 199−204.
(3) Mao, K.; Pruski, M. *J. Magn. Reson.* **2009**, *201*, 165−174.
(4) Walker, T. G. *J. Phys. Conf. Ser.* **2011**, *294*, 012001.
(5) Duckett, S. B.; Mewis, R. E. *Acc. Chem. Res.* **2012**, *45*, 1247−1257.
(6) Lawler, R. G. *Acc. Chem. Res.* **1972**, *5*, 25−33.
(7) Overhauser, A. W. *Phys. Rev.* **1953**, *92*, 411−415.
(8) Carver, T. R.; Slichter, C. P. *Phys. Rev.* **1953**, *92*, 212−213.
(9) Mak-Jurkauskas, M. L.; Griffin, R. G. High-Frequency Dynamic Nuclear Polarization. In *eMagRes*; John Wiley & Sons, Ltd., 2010; DOI: 10.1002/9780470034590.emrstm1183.
(10) Günther, U. L. In *Modern NMR Methodology*; Heise, H., Matthews, S., Eds.; Springer Berlin Heidelberg: Berlin, Heidelberg, Germany, 2013; pp 23−69.
(11) Lilly Thankamony, A. S.; Wittmann, J. J.; Kaushik, M.; Corzilius, B. *Prog. Nucl. Magn. Reson. Spectrosc.* **2017**, *102*, 120−195.
(12) Abragam, A.; Borghini, M.; Catillon, P.; Coustham, J.; Roubeau, P.; Thirion, J. *Phys. Lett.* **1962**, *2*, 310−311.
(13) Wind, R. A.; Duijvestijn, M. J.; van der Lugt, C.; Manenschijn, A.; Vriend, J. *Prog. Nucl. Magn. Reson. Spectrosc.* **1985**, *17*, 33−67.
(14) Becerra, L. R.; Gerfen, G. J.; Temkin, R. J.; Singel, D. J.; Griffin, R. G. *Phys. Rev. Lett.* **1993**, *71*, 3561−3564.
(15) Gerfen, G. J.; Becerra, L. R.; Hall, D. A.; Griffin, R. G.; Temkin, R. J.; Singel, D. J. *J. Chem. Phys.* **1995**, *102*, 9494−9497.
(16) Ardenkjaer-Larsen, J. H.; Fridlund, B.; Gram, A.; Hansson, G.; Hansson, L.; Lerche, M. H.; Servin, R.; Thaning, M.; Golman, K. *Proc. Natl. Acad. Sci. U. S. A.* **2003**, *100*, 10158−10163.
(17) Jóhannesson, H.; Macholl, S.; Ardenkjaer-Larsen, J. H. *J. Magn. Reson.* **2009**, *197*, 167−175.
(18) Jannin, S.; Bornet, A.; Melzi, R.; Bodenhausen, G. *Chem. Phys. Lett.* **2012**, *549*, 99−102.
(19) Cheng, T.; Capozzi, A.; Takado, Y.; Balzan, R.; Comment, A. *Phys. Chem. Chem. Phys.* **2013**, *15*, 20819−20822.
(20) Milani, J.; Vuichoud, B.; Bornet, A.; Miéville, P.; Mottier, R.; Jannin, S.; Bodenhausen, G. *Rev. Sci. Instrum.* **2015**, *86*, 024101.
(21) Batel, M.; Krajewski, M.; Weiss, K.; With, O.; Däpp, A.; Hunkeler, A.; Gimersky, M.; Pruessmann, K. P.; Boesiger, P.; Meier, B. H.; Kozerke, S.; Ernst, M. *J. Magn. Reson.* **2012**, *214*, 166−174.
(22) Bornet, A.; Melzi, R.; Perez Linde, A. J.; Hautle, P.; van den Brandt, B.; Jannin, S.; Bodenhausen, G. *J. Phys. Chem. Lett.* **2013**, *4*, 111−114.
(23) Batel, M.; Dapp, A.; Hunkeler, A.; Meier, B. H.; Kozerke, S.; Ernst, M. *Phys. Chem. Chem. Phys.* **2014**, *16*, 21407−21416.
(24) Nelson, S. J.; Kurhanewicz, J.; Vigneron, D. B.; Larson, P. E. Z.; Harzstark, A. L.; Ferrone, M.; van Criekinge, M.; Chang, J. W.; Bok, R.; Park, I.; Reed, G.; Carvajal, L.; Small, E. J.; Munster, P.; Weinberg, V. K.; Ardenkjaer-Larsen, J. H.; Chen, A. P.; Hurd, R. E.; Odegardstuen, L.-I.; Robb, F. J.; et al. *Sci. Transl. Med.* **2013**, *5*, 198ra108−198ra108.
(25) Joo, C.-G.; Hu, K.-N.; Bryant, J. A.; Griffin, R. G. *J. Am. Chem. Soc.* **2006**, *128*, 9428−9432.
(26) Sharma, M.; Janssen, G.; Leggett, J.; Kentgens, A. P. M.; van Bentum, P. J. M. *J. Magn. Reson.* **2015**, *258*, 40−48.
(27) Leggett, J.; Hunter, R.; Granwehr, J.; Panek, R.; Perez-Linde, A. J.; Horsewill, A. J.; McMaster, J.; Smith, G.; Kockenberger, W. *Phys. Chem. Chem. Phys.* **2010**, *12*, 5883−5892.
(28) Yoon, D.; Soundararajan, M.; Caspers, C.; Braunmueller, F.; Genoud, J.; Alberti, S.; Ansermet, J.-P. *J. Magn. Reson.* **2016**, *270*, 142−146.

DOI: 10.1021/acs.analchem.7b05236
Anal. Chem. 2018, 90, 3639−3650

(29) Rosay, M.; Blank, M.; Engelke, F. *J. Magn. Reson.* **2016**, *264*, 88−98.
(30) Prandolini, M. J.; Denysenkov, V. P.; Gafurov, M.; Lyubenova, S.; Endeward, B.; Bennati, M.; Prisner, T. F. *Appl. Magn. Reson.* **2008**, *34*, 399.
(31) Valentine, K. G.; Mathies, G.; Bédard, S.; Nucci, N. V.; Dodevski, I.; Stetz, M. A.; Can, T. V.; Griffin, R. G.; Wand, A. J. *J. Am. Chem. Soc.* **2014**, *136*, 2800−2807.
(32) Prisner, T.; Denysenkov, V.; Sezer, D. *J. Magn. Reson.* **2016**, *264*, 68−77.
(33) Liu, G.; Levien, M.; Karschin, N.; Parigi, G.; Luchinat, C.; Bennati, M. *Nat. Chem.* **2017**, *9*, 676−680.
(34) Reese, M.; Türke, M.-T.; Tkach, I.; Parigi, G.; Luchinat, C.; Marquardsen, T.; Tavernier, A.; Höfer, P.; Engelke, F.; Griesinger, C.; Bennati, M. *J. Am. Chem. Soc.* **2009**, *131*, 15086−15087.
(35) Barnes, A. B.; De Paëpe, G.; van der Wel, P. C. A.; Hu, K.-N.; Joo, C.-G.; Bajaj, V. S.; Mak-Jurkauskas, M. L.; Sirigiri, J. R.; Herzfeld, J.; Temkin, R. J.; Griffin, R. G. *Appl. Magn. Reson.* **2008**, *34*, 237−263.
(36) Zagdoun, A.; Rossini, A. J.; Gajan, D.; Bourdolle, A.; Ouari, O.; Rosay, M.; Maas, W. E.; Tordo, P.; Lelli, M.; Emsley, L.; Lesage, A.; Coperet, C. *Chem. Commun.* **2012**, *48*, 654−656.
(37) Lesage, A.; Lelli, M.; Gajan, D.; Caporini, M. A.; Vitzthum, V.; Miéville, P.; Alauzun, J.; Roussey, A.; Thieuleux, C.; Mehdi, A.; Bodenhausen, G.; Coperet, C.; Emsley, L. *J. Am. Chem. Soc.* **2010**, *132*, 15459−15461.
(38) Song, C.; Hu, K.-N.; Joo, C.-G.; Swager, T. M.; Griffin, R. G. *J. Am. Chem. Soc.* **2006**, *128*, 11385−11390.
(39) Sauvée, C.; Rosay, M.; Casano, G.; Aussenac, F.; Weber, R. T.; Ouari, O.; Tordo, P. *Angew. Chem., Int. Ed.* **2013**, *52*, 10858−10861.
(40) Zagdoun, A.; Casano, G.; Ouari, O.; Schwarzwälder, M.; Rossini, A. J.; Aussenac, F.; Yulikov, M.; Jeschke, G.; Copéret, C.; Lesage, A.; Tordo, P.; Emsley, L. *J. Am. Chem. Soc.* **2013**, *135*, 12790−12797.
(41) Sauvée, C.; Casano, G.; Abel, S.; Rockenbauer, A.; Akhmetzyanov, D.; Karoui, H.; Siri, D.; Aussenac, F.; Maas, W.; Weber, R. T.; Prisner, T.; Rosay, M.; Tordo, P.; Ouari, O. *Chem. - Eur. J.* **2016**, *22*, 5598−5606.
(42) Hu, K.-N.; Yu, H.-h.; Swager, T. M.; Griffin, R. G. *J. Am. Chem. Soc.* **2004**, *126*, 10844−10845.
(43) Matsuki, Y.; Maly, T.; Ouari, O.; Karoui, H.; Le Moigne, F.; Rizzato, E.; Lyubenova, S.; Herzfeld, J.; Prisner, T.; Tordo, P.; Griffin, R. G. *Angew. Chem., Int. Ed.* **2009**, *48*, 4996−5000.
(44) Zagdoun, A.; Casano, G.; Ouari, O.; Lapadula, G.; Rossini, A. J.; Lelli, M.; Baffert, M.; Gajan, D.; Veyre, L.; Maas, W. E.; Rosay, M.; Weber, R. T.; Thieuleux, C.; Coperet, C.; Lesage, A.; Tordo, P.; Emsley, L. *J. Am. Chem. Soc.* **2012**, *134*, 2284−2291.
(45) Kubicki, D. J.; Casano, G.; Schwarzwalder, M.; Abel, S.; Sauvee, C.; Ganesan, K.; Yulikov, M.; Rossini, A. J.; Jeschke, G.; Coperet, C.; Lesage, A.; Tordo, P.; Ouari, O.; Emsley, L. *Chem. Sci.* **2016**, *7*, 550−558.
(46) Can, T. V.; Caporini, M. A.; Mentink-Vigier, F.; Corzilius, B.; Walish, J. J.; Rosay, M.; Maas, W. E.; Baldus, M.; Vega, S.; Swager, T. M.; Griffin, R. G. *J. Chem. Phys.* **2014**, *141*, 064202.
(47) Mathies, G.; Caporini, M. A.; Michaelis, V. K.; Liu, Y.; Hu, K.-N.; Mance, D.; Zweier, J. L.; Rosay, M.; Baldus, M.; Griffin, R. G. *Angew. Chem., Int. Ed.* **2015**, *54*, 11770−11774.
(48) Thurber, K.; Tycko, R. *J. Chem. Phys.* **2014**, *140*, 184201.
(49) Mentink-Vigier, F.; Paul, S.; Lee, D.; Feintuch, A.; Hediger, S.; Vega, S.; De Paepe, G. *Phys. Chem. Chem. Phys.* **2015**, *17*, 21824−21836.
(50) Pinto, L. F.; Marin-Montesinos, I.; Lloveras, V.; Munoz-Gomez, J. L.; Pons, M.; Veciana, J.; Vidal-Gancedo, J. *Chem. Commun.* **2017**, *53*, 3757−3760.
(51) Lee, D.; Bouleau, E.; Saint-Bonnet, P.; Hediger, S.; De Paëpe, G. *J. Magn. Reson.* **2016**, *264*, 116−124.
(52) Thurber, K.; Tycko, R. *J. Magn. Reson.* **2016**, *264*, 99−106.
(53) Akbey, Ü.; Linden, A. H.; Oschkinat, H. *Appl. Magn. Reson.* **2012**, *43*, 81−90.
(54) Lelli, M.; Chaudhari, S. R.; Gajan, D.; Casano, G.; Rossini, A. J.; Ouari, O.; Tordo, P.; Lesage, A.; Emsley, L. *J. Am. Chem. Soc.* **2015**, *137*, 14558−14561.
(55) Chaudhari, S. R.; Berruyer, P.; Gajan, D.; Reiter, C.; Engelke, F.; Silverio, D. L.; Coperet, C.; Lelli, M.; Lesage, A.; Emsley, L. *Phys. Chem. Chem. Phys.* **2016**, *18*, 10616−10622.
(56) Chaudhari, S. R.; Wisser, D.; Pinon, A. C.; Berruyer, P.; Gajan, D.; Tordo, P.; Ouari, O.; Reiter, C.; Engelke, F.; Copéret, C.; Lelli, M.; Lesage, A.; Emsley, L. *J. Am. Chem. Soc.* **2017**, *139*, 10609−10612.
(57) Yarava, J. R.; Chaudhari, S. R.; Rossini, A. J.; Lesage, A.; Emsley, L. *J. Magn. Reson.* **2017**, *277*, 149−153.
(58) Lee, D.; Chaudhari, S. R.; De Paëpe, G. *J. Magn. Reson.* **2017**, *278*, 60−66.
(59) Bowen, S.; Hilty, C. *Phys. Chem. Chem. Phys.* **2010**, *12*, 5766−5770.
(60) Chen, H.-Y.; Hilty, C. *ChemPhysChem* **2015**, *16*, 2646−2652.
(61) Zeng, H.; Bowen, S.; Hilty, C. *J. Magn. Reson.* **2009**, *199*, 159−165.
(62) Frydman, L.; Blazina, D. *Nat. Phys.* **2007**, *3*, 415−419.
(63) Giraudeau, P.; Shrot, Y.; Frydman, L. *J. Am. Chem. Soc.* **2009**, *131*, 13902−13903.
(64) Guduff, L.; Kurzbach, D.; van Heijenoort, C.; Abergel, D.; Dumez, J.-N. *Chem. - Eur. J.* **2017**, *23*, 16722−16727.
(65) Ardenkjaer-Larsen, J. H.; Leach, A. M.; Clarke, N.; Urbahn, J.; Anderson, D.; Skloss, T. W. *NMR Biomed.* **2011**, *24*, 927−932.
(66) Lumata, L.; Ratnakar, S. J.; Jindal, A.; Merritt, M.; Comment, A.; Malloy, C.; Sherry, A. D.; Kovacs, Z. *Chem. - Eur. J.* **2011**, *17*, 10825−10827.
(67) Lumata, L.; Merritt, M.; Khemtong, C.; Ratnakar, S. J.; van Tol, J.; Yu, L.; Song, L.; Kovacs, Z. *RSC Adv.* **2012**, *2*, 12812−12817.
(68) Harris, T.; Bretschneider, C.; Frydman, L. *J. Magn. Reson.* **2011**, *211*, 96−100.
(69) Miéville, P.; Ahuja, P.; Sarkar, R.; Jannin, S.; Vasos, P. R.; Gerber-Lemaire, S.; Mishkovsky, M.; Comment, A.; Gruetter, R.; Ouari, O.; Tordo, P.; Bodenhausen, G. *Angew. Chem., Int. Ed.* **2010**, *49*, 6182−6185.
(70) Gajan, D.; Bornet, A.; Vuichoud, B.; Milani, J.; Melzi, R.; van Kalkeren, H. A.; Veyre, L.; Thieuleux, C.; Conley, M. P.; Grüning, W. R.; Schwarzwälder, M.; Lesage, A.; Copéret, C.; Bodenhausen, G.; Emsley, L.; Jannin, S. *Proc. Natl. Acad. Sci. U. S. A.* **2014**, *111*, 14693−14697.
(71) Carravetta, M.; Levitt, M. H. *J. Am. Chem. Soc.* **2004**, *126*, 6228−6229.
(72) Vasos, P. R.; Comment, A.; Sarkar, R.; Ahuja, P.; Jannin, S.; Ansermet, J.-P.; Konter, J. A.; Hautle, P.; van den Brandt, B.; Bodenhausen, G. *Proc. Natl. Acad. Sci. U. S. A.* **2009**, *106*, 18469−18473.
(73) Ji, X.; Bornet, A.; Vuichoud, B.; Milani, J.; Gajan, D.; Rossini, A. J.; Emsley, L.; Bodenhausen, G.; Jannin, S. *Nat. Commun.* **2017**, *8*, 13975.
(74) Gupta, R.; Lu, M.; Hou, G.; Caporini, M. A.; Rosay, M.; Maas, W.; Struppe, J.; Suiter, C.; Ahn, J.; Byeon, I.-J. L.; Franks, W. T.; Orwick-Rydmark, M.; Bertarello, A.; Oschkinat, H.; Lesage, A.; Pintacuda, G.; Gronenborn, A. M.; Polenova, T. *J. Phys. Chem. B* **2016**, *120*, 329−339.
(75) Fricke, P.; Demers, J.-P.; Becker, S.; Lange, A. *ChemPhysChem* **2014**, *15*, 57−60.
(76) Frederick, K. K.; Michaelis, V. K.; Corzilius, B.; Ong, T.-C.; Jacavone, A. C.; Griffin, R. G.; Lindquist, S. *Cell* **2015**, *163*, 620−628.
(77) Lelli, M.; Gajan, D.; Lesage, A.; Caporini, M. A.; Vitzthum, V.; Miéville, P.; Héroguel, F.; Rascón, F.; Roussey, A.; Thieuleux, C.; Boualleg, M.; Veyre, L.; Bodenhausen, G.; Coperet, C.; Emsley, L. *J. Am. Chem. Soc.* **2011**, *133*, 2104−2107.
(78) Romanenko, I.; Gajan, D.; Sayah, R.; Crozet, D.; Jeanneau, E.; Lucas, C.; Leroux, L.; Veyre, L.; Lesage, A.; Emsley, L.; Lacôte, E.; Thieuleux, C. *Angew. Chem., Int. Ed.* **2015**, *54*, 12937−12941.
(79) Ong, T.-C.; Liao, W.-C.; Mougel, V.; Gajan, D.; Lesage, A.; Emsley, L.; Copéret, C. *Angew. Chem., Int. Ed.* **2016**, *55*, 4743−4747.
(80) Berruyer, P.; Lelli, M.; Conley, M. P.; Silverio, D. L.; Widdifield, C. M.; Siddiqi, G.; Gajan, D.; Lesage, A.; Copéret, C.; Emsley, L. *J. Am. Chem. Soc.* **2017**, *139*, 849−855.
(81) Lee, D.; Duong, N. T.; Lafon, O.; De Paëpe, G. *J. Phys. Chem. C* **2014**, *118*, 25065−25076.
(82) Perras, F. A.; Wang, Z.; Naik, P.; Slowing, I. I.; Pruski, M. *Angew. Chem., Int. Ed.* **2017**, *56*, 9165−9169.

DOI: 10.1021/acs.analchem.7b05236
Anal. Chem. 2018, 90, 3639−3650

(83) Ouari, O.; Phan, T.; Ziarelli, F.; Casano, G.; Aussenac, F.; Thureau, P.; Gigmes, D.; Tordo, P.; Viel, S. *ACS Macro Lett.* **2013**, *2*, 715−719.
(84) Pinon, A. C.; Rossini, A. J.; Widdifield, C. M.; Gajan, D.; Emsley, L. *Mol. Pharmaceutics* **2015**, *12*, 4146−4153.
(85) Rossini, A. J.; Widdifield, C. M.; Zagdoun, A.; Lelli, M.; Schwarzwälder, M.; Copéret, C.; Lesage, A.; Emsley, L. *J. Am. Chem. Soc.* **2014**, *136*, 2324−2334.
(86) Märker, K.; Pingret, M.; Mouesca, J.-M.; Gasparutto, D.; Hediger, S.; De Paëpe, G. *J. Am. Chem. Soc.* **2015**, *137*, 13796−13799.
(87) Märker, K.; Paul, S.; Fernandez-de-Alba, C.; Lee, D.; Mouesca, J.-M.; Hediger, S.; De Paëpe, G. *Chem. Sci.* **2017**, *8*, 974−987.
(88) Kobayashi, T.; Perras, F. A.; Goh, T. W.; Metz, T. L.; Huang, W.; Pruski, M. *J. Phys. Chem. Lett.* **2016**, *7*, 2322−2327.
(89) Kobayashi, T.; Perras, F. A.; Murphy, A.; Yao, Y.; Catalano, J.; Centeno, S. A.; Dybowski, C.; Zumbulyadis, N.; Pruski, M. *Dalton Trans.* **2017**, *46*, 3535−3540.
(90) Ardenkjaer-Larsen, J. H.; Laustsen, C.; Bowen, S.; Rizi, R. *Magn. Reson. Med.* **2014**, *71*, 50−56.
(91) Comment, A. *J. Magn. Reson.* **2016**, *264*, 39−48.
(92) Chappuis, Q.; Milani, J.; Vuichoud, B.; Bornet, A.; Gossert, A. D.; Bodenhausen, G.; Jannin, S. *J. Phys. Chem. Lett.* **2015**, *6*, 1674−1678.
(93) Min, H.; Sekar, G.; Hilty, C. *ChemMedChem* **2015**, *10*, 1559−1563.
(94) Buratto, R.; Bornet, A.; Milani, J.; Mammoli, D.; Vuichoud, B.; Salvi, N.; Singh, M.; Laguerre, A.; Passemard, S.; Gerber-Lemaire, S.; Jannin, S.; Bodenhausen, G. *ChemMedChem* **2014**, *9*, 2509−2515.
(95) Lee, Y.; Heo, G. S.; Zeng, H.; Wooley, K. L.; Hilty, C. *J. Am. Chem. Soc.* **2013**, *135*, 4636−4639.
(96) Bowen, S.; Hilty, C. *Angew. Chem., Int. Ed.* **2008**, *47*, 5235−5237.
(97) Jensen, P. R.; Meier, S.; Ardenkjaer-Larsen, J. H.; Duus, J. O.; Karlsson, M.; Lerche, M. H. *Chem. Commun.* **2009**, 5168−5170.
(98) Miclet, E.; Abergel, D.; Bornet, A.; Milani, J.; Jannin, S.; Bodenhausen, G. *J. Phys. Chem. Lett.* **2014**, *5*, 3290−3295.
(99) Bornet, A.; Ji, X.; Mammoli, D.; Vuichoud, B.; Milani, J.; Bodenhausen, G.; Jannin, S. *Chem. - Eur. J.* **2014**, *20*, 17113−17118.
(100) Allouche-Arnon, H.; Gamliel, A.; Sosna, J.; Gomori, J. M.; Katz-Brull, R. *Chem. Commun.* **2013**, *49*, 7076−7078.
(101) Allouche-Arnon, H.; Hovav, Y.; Friesen-Waldner, L.; Sosna, J.; Moshe Gomori, J.; Vega, S.; Katz-Brull, R. *NMR Biomed.* **2014**, *27*, 656−662.
(102) Lerche, M. H.; Meier, S.; Jensen, P. R.; Hustvedt, S.-O.; Karlsson, M.; Duus, J. Ø.; Ardenkjaer-Larsen, J. H. *NMR Biomed.* **2011**, *24*, 96−103.
(103) Dumez, J.-N.; Milani, J.; Vuichoud, B.; Bornet, A.; Lalande-Martin, J.; Tea, I.; Yon, M.; Maucourt, M.; Deborde, C.; Moing, A.; Frydman, L.; Bodenhausen, G.; Jannin, S.; Giraudeau, P. *Analyst* **2015**, *140*, 5860−5863.
(104) Bornet, A.; Maucourt, M.; Deborde, C.; Jacob, D.; Milani, J.; Vuichoud, B.; Ji, X.; Dumez, J.-N.; Moing, A.; Bodenhausen, G.; Jannin, S.; Giraudeau, P. *Anal. Chem.* **2016**, *88*, 6179−6183.
(105) Lerche, M. H.; Yigit, D.; Frahm, A. B.; Ardenkjaer-Larsen, J. H.; Malinowski, R. M.; Jensen, P. R. *Anal. Chem.* **2018**, *90*, 674−678.

DOI: 10.1021/acs.analchem.7b05236
Anal. Chem. 2018, 90, 3639−3650